DOI 10.1007/s11041-022-00796-9
Metal Science and Heat Treatment, Vol. 64, Nos. 5 – 6, September, 2022 (Russian Original Nos. 5 – 6, May – June, 2022)

CHEMICAL HEAT TREATMENT AND COATINGS

UDC 538.911:621.791:621.001.57

MODELING BY A MOLECULAR DYNAMICS METHOD OF STRUCTURAL CHANGES OF A BCC METAL SURFACE LAYER WITH SHORT-TERM HIGH-ENERGY EXTERNAL ACTION

A. V. Markidonov,[1] M. D. Starostenkov,[2] A. N. Gostevskaya,[3] D. A. Lubyanoy,[4] and P. V. Zakharov[5]

Translated from *Metallovedenie i Termicheskaya Obrabotka Metallov*, No. 5, pp. 16 – 21, May, 2022.

Original article submitted January 11, 2022.

Results of molecular-dynamic simulation of structural changes in the surface layer of a design cell of a BCC-crystal under short-term high-energy action are presented. A spatial model where the temperature of the design cell is distributed in accordance with the solution of a linear problem of heat conduction makes it possible to detect disruption of surface layer continuity, including localization of excess free volumes in the form of spherical pores. Dimensions of these imperfections and the time of their existence differ during modeling of laser radiation with different energy density. Conditions are revealed for pore stability during the whole simulation period and a relationship between crystallographic orientation of the "solid – liquid" interphase boundary and sizes of pores formed is determined.

Keywords: crystal, model, temperature, melting, pore, surface, interphase boundary.

INTRODUCTION

As a result of action on metal of ultrashort highly powerful laser pulses unique physical conditions are created, i.e., a fast material heating rate and a volumetric mechanism of laser radiation energy liberation. All of this leads to a situation that a solid body is heated to a temperature exceeding an equilibrium value for both melting temperature and evaporation temperature. Picosecond laser pulses with respect to operation duration are comparable with temperatures and phases for transformations within material. However, the thermal effect of pulses outside their action zone is at a minimum. It is undoubted that processes of equilibrium substance heating during laser treatment are of practical interest and therefore they serve as an object for various experimental and theoretical studies [1 – 3].

Material irradiation with high power laser pulses may lead to melting and melt movement caused by sharp temperature gradients and pressure relaxation, with subsequent substance separation from a surface (ablation) that has its own application in various regions. The phenomenon of ablation by laser is studied successfully by means of molecular dynamics [4 – 6], although a whole series of assumptions are made. For example, within the framework of classical molecular dynamics it is necessary to consider time intervals corresponding to typical time of electron-phonon relaxation.

Structural changes proceeding within an amorphous phase in the cooling stage after the end of action undoubtedly have an effect on the properties of an entirely or partly crystallized structure. In this connection a study of material amorphous structure subjected to laser action is of practical interest.

[1] Kuzbass Humanitarian Pedagogical Institute of the Kuzbass State University, Novokuznetsk, Russia.
[2] I. I. Polzunov Altai State Technical University, Barnaul, Russia.
[3] Siberian State Industrial University, Novokuznetsk, Russia (e-mail: lokon1296@mail.ru).
[4] T. F. Gorbachev branch of the Kuzbass State Technical University, Prokop'evsk, Russia.
[5] Peter the Great St. Petersburg Polytechnic University, St. Petersburg, Russia.

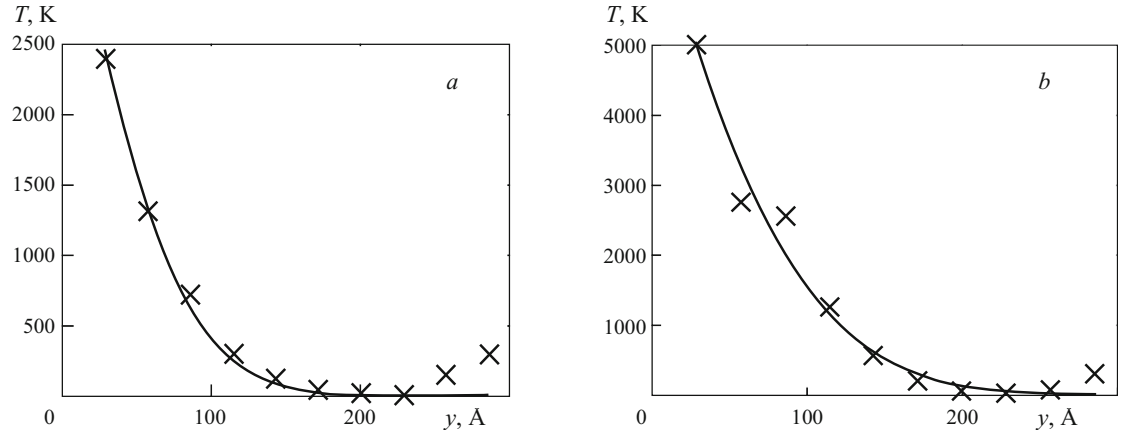

Fig. 1. Calculated temperature change (solid line) through crystal thickness (y is distance over surface for axis Y) and average layer temperature values of a design cell through 1 psec (*a*) and 12 psec (*b*) of model time. Modeled laser radiation energy density $q = 3.5$ MW/cm^2.

The aim of the present work is to study structural changes proceeding within material during high-temperature laser action within the scope of molecular-dynamic modeling.

METHODS OF STUDY

A model has been developed as follows. Within a rectangular coordinate system the size of a calculation cell was prescribed in three mutually orthogonal crystallographic directions coinciding with coordinate axes. Then an experimental cell was constructed within which particle location corresponded to an FCC lattice. Such cells fill all of a prescribed volume by translation. A calculation cell is a rectangular parallelepiped with a side ratio $(20 \times 100 \times 12) \times a_0$, where a_0 is metal lattice spacing in an equilibrium condition. Since it has been proposed to conduct a study on an iron crystal model then its lattice spacing has been prescribed equal to 2.866 Å. The overall number of molecular particles is 48,000. Along the X and Z axes periodic boundary conditions have been used, and along the Y axis there are free conditions simulating a crystal surface. The orientation of the calculation cell within space was selected in order that the X-axis coincides with the crystallographic direction [100], axis Y with direction [010], and axis Z with direction [001]. A potential was used as a function of the interparticle reaction built up by the submerged atom method [7]. In order to integrate movement equations describing behavior of a particle system a Verlet velocity algorithm was used with a time step of 1 fsec. Calculations were performed using an XMD package. Visualization of modeling results was accomplished by means of an OVITO package [8].

In order to model target heating under action of laser radiation a calculation cell was broken down into ten layers of equal thickness along axis Y in each of which a specific temperature value was prescribed decreasing on removal from the surface. During establishment of thermal equilibrium between electrons and phonons in order to described heat distribution it is possible to use a thermal conductivity model. With use of a semicontinuous solid model an analytically precise solution of the thermal problem may be obtained integral transformations [9]. In this case if the source intensity depends on time and physical parameters are constant and do not depend upon temperature (linear thermal conductivity problem), then the temperature distribution though a specimen thickness in the heating stage is determined as a function of coordinates as follows (with $t < \tau$):

$$T(y, t) = \frac{2Aq}{\lambda}\sqrt{at} \times ierfc\left(\frac{y}{2\sqrt{at}}\right), \quad (1)$$

where T is temperature; y is coordinate; t is current time; A is absorption capacity; q is energy density; λ is heat conduction; a is thermal conductivity thermal conductivity; $a = \lambda/\rho C$); τ is radiation action duration.

Function $ierfc(x)$, present within Eq. (1), is an integral of the probability interval function:

$$ierfc(x) = \int_x^\infty erfc(x)\mathrm{d}x. \quad (2)$$

After the end of laser activity ($t < \tau$) a cooling stage sets in and temperature distribution is described by an equation

$$T(y, t) = \frac{2Aq}{\lambda} \times \left[\sqrt{at} \times ierfc\left(\frac{y}{2\sqrt{at}}\right) - \sqrt{a(t-\tau)} \times ierfc\left(\frac{y}{2\sqrt{a(t-\tau)}}\right)\right]. \quad (3)$$

In order to calculate temperature the following parameters were used: $A = 0.68$; $q = 3.0 - 6.5$ mW/cm^2; $\lambda = 80$ W/m · K; $a = 2.621 \times 10^{-5}$ m^2/sec; $\tau = 1 \times 10^{-12}$ sec.

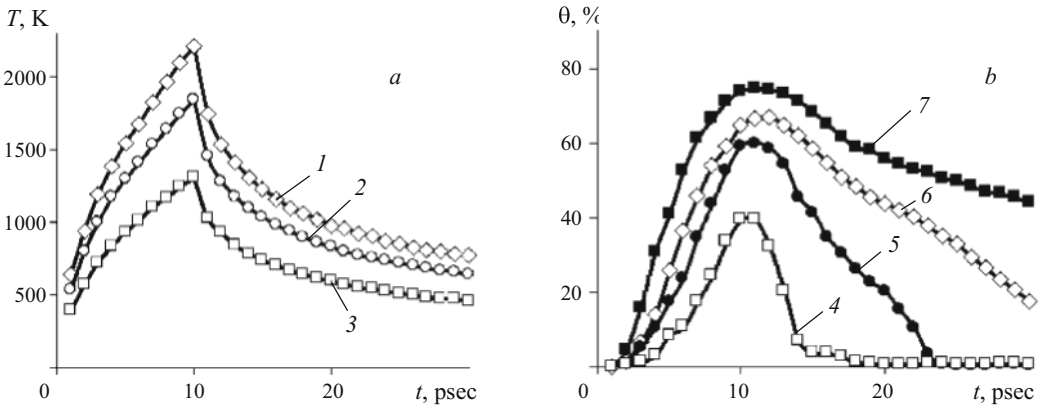

Fig. 2. Change in average temperature (*a*) and porosity coefficient (*b*) of design cell during laser radiation with different energy density: *1*) $q = 3.5$ MW/cm^2; *2*) $q = 5.0$ MW/cm^2; *3*) $q = 6.5$ MW/cm^2; *4*) $q = 3.0$ MW/cm^2; *5*) $q = 3.5$ MW/cm^2; *6*) $q = 4.0$ MW/cm^2; *7*) $q = 4.0$ MW/cm^2.

Non-equilibrium heating of a model specimen may lead formation of a compression region close to its surface propagating inwards in the form of a pressure wave. This wave, reaching the opposite boundary, with use of free boundary conditions will cause particle movement. In order to avoid this in a layer most distant from the model surface, by means of a thermostatic control procedure a constant temperature of 300 K was maintained and also ductile boundary conditions were superimposed.

Theoretical curves are provided in Fig. 1 for the change in temperature within a specimen along axis *Y*, calculated by Eq. (1), and values of temperature within separate layers of a calculation cell. It is seen that for the layers most distant from a surface the calculated and experimental temperature values obtained for are different. This is due to use of a thermostatic control procedure described above. In view of this the structure of lower layers was considered in the work.

RESULTS AND DISCUSSION

The modeling process consisted of two stages. In the initial stage a calculation cell was subjected to non-equilibrium heating for 10 psec of model time in accordance with Eq. (1). After which a second phase follows including nonequilibrium cooling for 20 psec, with which the temperature of the calculation cell was established in accordance with Eq. (3). A change is given in Fig. 2*a* for the average temperature of the calculation cell under action of laser radiation.

After the design cell local temperature in the heating stage starts to exceed the melting temperature, there is phase transformation and within a cell a solid and liquid phase interface forms moving into a lower temperature region. The next increase in temperature leads to a situation that particles start to separate from the surface of the design cell forming a cloud of evaporated particles. The cooling stage is accompanied by localization of the rarefaction regions formed in the preceding heating stage (Fig. 3*a*), their coalescence and spherical pores formation (Fig. 3*b* – *d*).

In order to identify cavities and to evaluate their surface area in subsequent calculations an algorithm [10] is used based on the alpha-form procedure of G. Edelsbrunner and E. Myukke, within which a geometric multiplicity of points is connected with a surface network by beams of a Delaunay tetrahedralization and a subsequent smoothing procedure. Identification of cavities within the volume of a solid is determined by the radius of a virtual sphere which is inscribed within interatomic space. The radius of this sphere should exceed to a minimum half the shortest interatomic distance, otherwise within calculations "artificial" cavities will be included. In this work the radius of a virtual sphere equals the value of the lattice spacing.

During modeling of different radiation absorption density, achieved by variation of parameter q in Eqs. (1) and (3), structural changes are observed within design cell surface layers. As a rule for quantitative evaluation of a similar type of change a velocity coefficient is used expressed in terms of an amorphous and crystalline structure. In our case a clearer porosity coefficient θ, determined as the proportion of free surface created by pores, is within the overall free surface identified within the calculation cell. Curves are provided in Fig. 2*b* for the change in θ during laser radiation with different q obtained by the model proposed.

As follows from Fig. 2*b*, with $q \le 3.5$ mW/cm^2 cavities formed with a cell in accordance with the model proposed are dissolved. With higher q values in the amorphous region there is formation of extended cavities remaining stable over the whose extent of modeling. A similar type of defect will be the object for study by the authors in subsequent work.

The pore dissolution mechanism within a design cell surface layer is a material diffusion viscous flow within a formed cavity. Irregular occurrence of diffusion processes is mainly determined by temperature and consequently pore stability in the second modeling stage will depend upon the

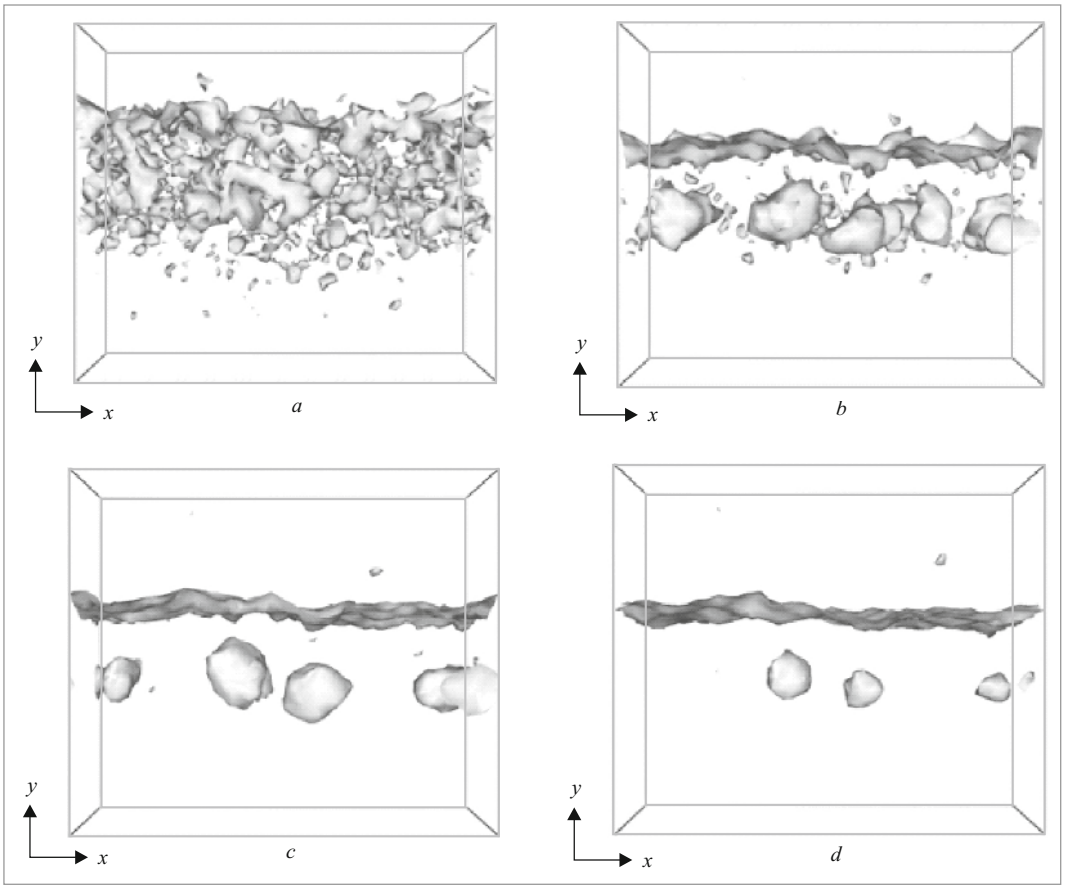

Fig. 3. Visualization of a free surface formed within a design cell (a fragment is presented), through 11 psec (*a*), 15 psec (*b*), 19 psec (*c*) and 22 psec (*d*) of model time. Laser radiation modelled density $q = 3.5$ MW/cm^2.

design cell cooling rate. With implementation of cooling in accordance with Eq. (3) thus rate is evaluated as 3.53×10^{13} K/sec. In order to achieve other rates in Eq. (3) coefficient $(\tau/t)^n$ is added, where n is an arbitrary rational number. With variation of n faster cooling rates have been obtained with which porosity of upper layers is retained. Modeling results are provided in Fig. 4.

It should be noted that from the point of view of a quasi-thermodynamic approach for describing new phase formation within a condensed medium formation of fluctuation by means of pore generation is hardly probable (phase cavities) with a size exceeding some critical value determined by specific surface energy. In view of this for homogeneous pore generation elastic tensile tresses are required whose source may be excess vacancies [11]. Another source of stresses within a solid may be an impact wave [12 – 14]. In our case the stressed state of a design cell is due to nonuniform heating and moreover the interface creates the stress field observed whose value is proportional to free surface energy γ. Free energy of the crystal – melt separation boundary is anisotropic and it depends upon solid phase crystal orientation [15]. In this case as follows from results in [16] for a BCC structure anisotropy develops to a much lesser extent than for FCC. In addition, the authors of [17], making calculations of iron free surface energy anisotropy by means of various research methods have obtained results having scatter of the order to 5%. However, if these data are analyzed it

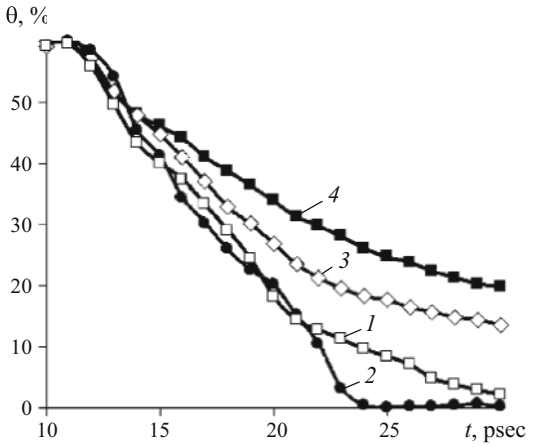

Fig. 4. Change in calculated cell strength coefficient θ in the concluding stage of modeling with a different cooling rate (modeling laser radiation energy density $q = 3.5$ MW/cm^2): *1*) 3.53×10^{13} K/sec; *2*) 4.39×10^{13} K/sec; *3*) 4.62×10^{13} K/sec; *4*) 4.77×10^{13} K/sec.

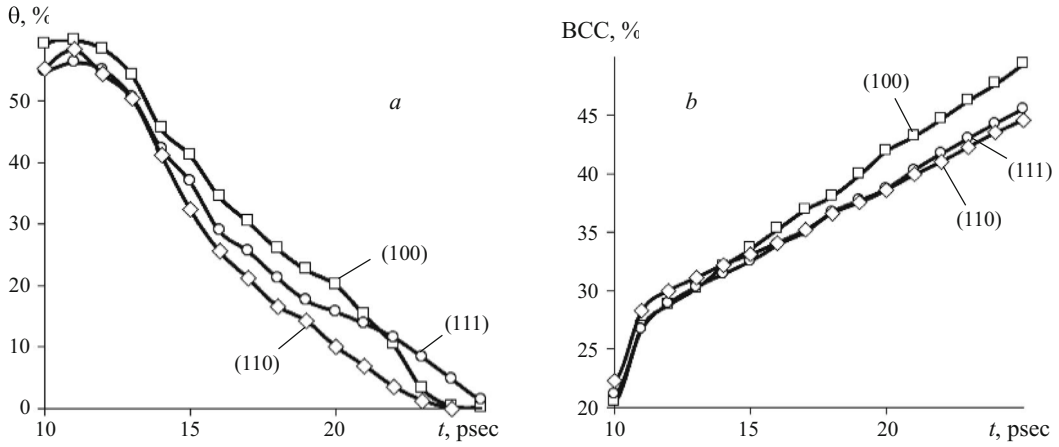

Fig. 5. Change in design cell porosity coefficient θ (*a*) and proportion of BCC atoms with local FCC-surrounding (*b*) in modeling concluding stage with crystallographic orientation of interphase boundary along (100), (111), (110).

may be concluded that the ratio $\gamma_{110} \leq \gamma_{111} < \gamma_{100}$ is valid. Consequently, the higher the reticulated surface of a crystal plane, forming an interface, the lower is the iron free surface energy.

We have performed modeling of design cells containing interfaces of different crystallographic orientation. It appeared that the pore dimensions and their time for existence also vary, although the temperature of the upper layer during modeling interface boundaries of different crystallographic orientations changes very little. Results are shown in Fig. 5 for calculation of porosity coefficient in the cooling stage (within a time section containing the clearest result) analysis of data in Fig. 5*a* showed that there is an interconnection between crystallographic orientation of a boundary and sizes of the cavities formed, but it only appears clearly in a certain time interval. Apparently to the least extent the effect of a boundary starts to appear at that instant when in the process of its movement in the cooling stage of a design cell it approaches a vacancy. In this case the interphase boundary exhibiting greatest energy γ moves at the fastest rate. As a result of this densification of a surface layer there is a more intense and a larger amount of free volume localized in the form of pores and it does not dissolve. In accordance with this during modeling an interphase boundary with crystallographic orientation (100) there is formation of larger pores, but since cooling rate is identical, then in all cases they dissolve in approximately an equal time interval. Confirmation of this mechanism is the fact that proportion of atoms with local BCC-environment in all three upper layers during modeling an interphase boundary with orientation (100) in the cooling stage it increases much more rapidly compared with other boundary mode orientations (Fig. 5*b*). In this case in order to conduct structural analysis intensification of the local environment of particles is used employing an Ackland–Jones method of angles and bonds [18].

CONCLUSIONS

Rapidly occurring processes within solids are currently studied successfully by means of computer modeling methods. In the present work a molecular dynamic model is constructed for studying processes occurring within material surface layers with external short-term high-energy action. It has been detected that within a surface layer after the end of an external effect the free volume is localized in the form of groups of pores that dissolve in the shrinkage process. It is possible to stabilize these pores by increasing the cell cooling rate. The effect of interphase boundary "solid – liquid" orientation on the pore size formed has also been established.

Research results may find use in studying laser ablation and surface modification processes.

REFERENCES

1. M. A. Zav'yalova, "Surface modification of quartz glass by a pulsed picosecond laser," *Komp. Optika*, **40**(6), 863 – 870 (2016).
2. V. I. Mazhukin, M. NM. Demin, and A. V. Shapranov, "Effects of non-equilibrium with action of pulsed laser radiation on metal," *Opt. Zh.,* **78**(8), 29 – 37 (2011).
3. T. O. Yavtushenko, A. S. Kadochnikov, S. G. Novikov, et al., "Experimental study of structuring of a metal surface by high power femtosecond laser pulses," *Izvest. Samar. Nauch. Tsentra Ross. Akad. Nauk*, **15**[4(5)], 1033 – 1037 (2013).
4. J.-K. Kuo, P.-H. Huang, S.-K. Chien, et al., "Molecular dynamics simulations of crater formation induced by laser ablation on the surface of α-Fe substrate" *MATEC Web of Conferences*, **167**, No. 03011 (2018).
5. X.-F. Gong, G.-X. Yang, P. Li, et al., "Molecular dynamics simulation of pulsed laser ablation," *Int. J. Modern Phys. B*, **25**(4), 543 – 550 (2011).
6. C. Cheng, A. Q. Wu, and X. Xu, "Molecular dynamics simulation of ultrafast laser ablation of fused silica," *J. Phys.: Conf. Ser.*, **59**, 100 – 104 (2007).

7. M. I. Mendelev, S. Han, D. J. Srolovitz, et al., "Development of new interatomic potentials appropriate for crystalline and liquid iron," *Philos. Mag.*, **83**(35), 3977 – 3994 (2003).
8. A. Stukowski, "Visualization and analysis of atomistic simulation data with OVITO — the Open Visualization Tool," *Model. Simul. Mater. Sci. Eng.*, **18**, 015012 (2010).
9. N. N. Rykalkin, A. A. Uzlov, I. V. Zuev, and A. N. Kokora, *Laser and Electron Beam Treatment of Materials: Handbook* [in Russian], Mashinostroenie, Moscow (1985).
10. A. Stukowski, "Computational analysis methods in atomistic modeling of crystals," *J. Minerals, Met. & Mater. Soc.*, **66**(3), 399 – 407 (2014).
11. V. L. Orlov and A. G. Malyshkina, "Formation of nanometric ordered structures of radiation pores," *Izv. Vysh. Uchebn. Zaved., Fizika*, **46**(2), 31 – 35 (2003).
12. A. V. Markidonov and M. D. Starostenkov, "Possibility of homogeneous pore generation in grain boundary region under action impact post-cascade waves," *Vopr. Atom. Nauki Tekh., Ser. Matemat. Model. Fiz. Protsessov*, No. 3, 37 – 46 (2016).
13. A. V. Markidonov, M. D. Starostenkov, and E. P. Pavlovskaya, "Effect of post-cascade impact waves on vacancy pore coarsening," *Fund. Probl. Sovr. Mater.*, **9**(4-2), 694 – 701 (2012).
14. A. V. Markidonov, M. D. Starostenkov, and P. V. Zakharov, "Growth of small vacancy accumulations initiated by sliding post-cascade impact waves," *Pis'ma Mater.*, **2**(2), 111 – 114 (2012).
15. J. R. Morris and X. Song, "The anisotropic free energy of the Lennard-Jones crystal-melt interface," *J. Chem. Phys.*, **119**(7), 3920 – 3925 (2003).
16. D. Y. Sun, M. Asta, J. J. Hoyt, et al., "Crystal-melt interfacial free energies in metals: fcc versus bcc," *Phys. Rev. B*, **69**(2), 020102 (2004).
17. J. Liu, R. L. Davidchack, and H. B. Dong, "Molecular dynamics calculation of solid-liquid interfacial free energy and its anisotropy during iron solidification," *Comput. Mater. Sci.*, **74**, 92 – 100 (2013).
18. G. J. Ackland and A. P. Jones, "Applications of local crystal structure measures in experiment and simulation," *Phys. Rev. B*, **73**(5), 054104 (2006).